J Solid State Electrochem (2007) 11:1171–1182
DOI 10.1007/s10008-006-0257-1

ORIGINAL PAPER

Impedance modelling of two-phase solid-state ionic conductors. Part I—theoretical model and computer simulations

E. E. Horopanitis · G. Perentzis · L. Papadimitriou

Received: 26 June 2006 / Revised: 29 November 2006 / Accepted: 8 December 2006 / Published online: 16 January 2007

Abstract An equivalent circuit model is introduced to account for the impedance properties of solid state ionic conductors, composed of two distinct phases. The model is developed on the basis of physical arguments, regarding the micrometer-scale structure of the two-phase material system and the comparison of different possible equivalent circuit representations. The final equivalent circuit reduces to two simpler circuits, suitable for fitting experimental impedance spectra. Computer simulations are provided to demonstrate the non-Arrhenius behaviour, which is observed in the temperature dependence of the ohmic elements of the equivalent circuits used for data analysis. This complex dual-slope behaviour of the Arrhenius plot is in agreement with the predictions of the model. Finally, with the aid of mathematical calculations and illustrated by computer simulations, a modified Arrhenius plot evaluation procedure was developed to derive correctly the electrical properties of the individual constituent phases from impedance measurements.

Keywords Ionic conductivity · Impedance spectroscopy · Equivalent circuits · Two-phase materials

Introduction

Impedance spectroscopy is an electrical characterization technique that has been extensively employed for the study of solid materials and devices [1–3]. Impedance spectra are analysed by means of equivalent circuit models, which correlate the impedance of the experimental cell to the physical and structural properties of the materials making up the cell, and the geometry of their arrangement. Usually, there are more than one equivalent circuits that yield the same impedance frequency response [4] and may be used equally well for formal description of impedance spectra. The choice of a particular equivalent circuit among a set of alternatives may, therefore, greatly affect the quantitative results derived from impedance measurements, as well as the physical interpretation of the investigated phenomenon.

The aim of the present first part of this work is to introduce an equivalent circuit model to account for the shape of Arrhenius plots, which describe the variation of the conductivity of two-phase ionic conductors with temperature. The model is derived on the grounds of conclusions drawn from previous experiments [5], regarding the micrometer-scale structure of a class of vitreous boron-oxide-based lithium-ion conductors [2, 6, 7]. Under high lithium doping, boron oxide glass systems become inhomogeneous, with crystalline grains forming in the vitreous volume. Details are given elsewhere [5], as well as in the second part of this work. The model can easily be extended to any two-phase system in which one of the phases is distributed in the form of isolated islands within the background of the other phase.

The development of the model is described step-by-step, with emphasis placed on the physical reasoning that lies behind the assignment of each circuit element as a model to specific electrical response processes, as well as the interconnection of the elements in the circuit to describe the interrelation among these processes. A first approximation of the equivalent circuit is formulated from a purely technical point of view to account for the graphical components of the Nyquist plot. The circuit is subsequently

E. E. Horopanitis · G. Perentzis · L. Papadimitriou (✉)
Department of Physics, Section of Solid State Physics,
Aristotle University of Thessaloniki,
54124 Thessaloniki, Greece
e-mail: pleonida@auth.gr

refined accordingly on the basis of physical arguments and the comparison of typical impedance spectra fitting results obtained from the above-mentioned two-phase materials.

The model offers an explanation of the seemingly irregular non-Arrhenius behaviour observed in the temperature dependence of the ionic conductivity of the phases constituting the material under investigation [8]. Similar complex Arrhenius behaviour has been observed in past results, published by various researchers, regarding the grain boundary phase of polycrystalline ceramics [9–11]. We do not refer to the effect of non-Arrhenius temperature dependence of ionic conductivity that has been identified [12] in a series of fast-ion conducting glasses, implying conductivity saturation at high temperatures. This phenomenon has been observed in single-phase disordered materials [13], and all attempted explanations, so far, deal with the physics of ion transport processes [14–16], whereas we are concerned with material systems that are unmistakably composed of multiple phases, at temperatures well below the glass-transition temperature. Computer simulations are provided to the purpose of demonstrating the irregular dual-slope shape of Arrhenius plots, as constructed by customary impedance data fitting. Finally, a modified analysis procedure of Arrhenius plots, formulated by mathematical analysis, is presented, allowing correct calculation of the electrical properties of the individual phases making up the two-phase material, according to the predictions of the proposed equivalent circuit model.

To our knowledge, similar work has been reported only in the case of ion-conducting polycrystalline ceramics [9, 10, 17–22] in which the grain boundary phase forms a continuous network surrounding the individual crystalline grains. The earliest equivalent circuit models of ionic conductivity in the bulk of polycrystalline ceramics, attempting to relate electrical properties to microstructure, adopted directly, or reduced to, the series configuration of two resistor-capacitor pairs, each of which corresponded to grain interior and grain boundary phase conductivity [14, 17–21]. The observed similarity in the temperature dependence of conductivity in the two phases was explained by adding a constriction resistance in parallel to the grain boundary component of the circuit, and stating that ionic conduction through easy paths bypasses conduction through the highly resistive grain boundary phase [17]. Easy paths are formed by the connectivity of regions in the grain boundary phase, where good contact between grains is established. However, a study of the temperature dependence of circuit elements as a function of microstructural parameters was not presented. According to a different approach, applicable to cases in which the coverage of the grain boundary phase in the ceramic is low, part of the ionic current is capacitively blocked at grain boundaries [1, 23]. The easy paths principle was employed to explain the transition exhibited in the slope of the temperature dependence of conductivity [9, 10]. At low temperatures, easy path conduction bypasses grain boundary conduction, but as the temperature increases, grain boundary conduction prevails due to its higher activation energy [10]. An alternative equivalent circuit, consisting of several parallel branches identical to the previously mentioned series model, was proposed to study the effect of microstructural inhomogeneity and anisotropy on ionic conductivity [11]. More complex circuits were introduced to model constriction effects at the contact points between grains by considering variations in the current distribution at different frequencies. Nevertheless, it turned out that the circuits reduced to the same, widely applied circuits, in some of which, capacitances should simply be replaced by constant phase elements (CPEs) [24–26]. Only the interpretation of circuit elements depends on the details of the adopted microstructural model.

Fitting equivalent circuits to impedance spectra

A typical impedance spectrum in Nyquist representation of a two-phase solid state material, obtained from a $4Li_2O$–B_2O_3 glass sample [2, 5] at 81 °C, is shown in Fig. 1. The frequency explicit Bode plots of the real and imaginary parts of the impedance are contained in the same figure as insert plots. The spectrum consists of three graphical components, namely, two consecutive semicircular arcs in the high-frequency branch and a straight line in the low-frequency branch of the Nyquist plot. The components of the spectrum are also displayed in each one of the plots of Fig. 1. The low-frequency impedance response of the experimental cell is due to polarization effects of the

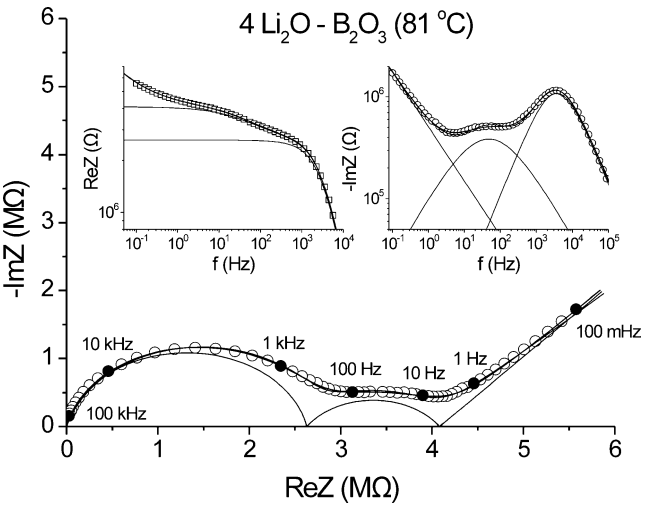

Fig. 1 Typical impedance spectrum in Nyquist and Bode representation (*insert plots*) of a two-phase material, obtained from a $4Li_2O$–B_2O_3 glass sample at 81 °C

interfaces between the sample and ion-blocking electrodes. The two arcs are due to equal in number electrical relaxation processes in the material. As earlier experiments [5] have demonstrated the presence of two phases, vitreous and crystalline, the two relaxation processes are attributed to the different properties of electrical conductivity in these phases [1]. Modelling the impedance properties of a two-phase material, then, reduces to the problem of selecting a suitable equivalent circuit, whose impedance response reproduces the two arcs.

The equivalent circuit that has been widely adopted to account for the impedance frequency response of the experimental cell intended for impedance measurements [27] is shown in Fig. 2. Its main component is a subcircuit that models the bulk electrical properties of the material under investigation. During experimental data fitting sessions, this subcircuit is replaced in the general circuit of Fig. 2 by the candidate equivalent circuits of the two-phase material that will be presented in the next sections. Capacitor C_g models the geometrical capacitance of the cell, which is usually disregarded due to its very small value. The constant phase element (CPE) Q_i models the impedance response of the interfaces between the sample and the electrodes. When inert metallic electrodes are used and any chemical activity at the interfaces is presumed to be absent, the most likely cause of the CPE-type interfacial behaviour is the geometrical effect of porous and rough electrodes [1, 28–31].

From a purely technical point of view, fitting an equivalent circuit to an impedance spectrum that presents two semicircular arcs in its Nyquist plot is attained by incorporating two resistors and two CPEs in the circuit under two conditions. First, the two resistors or CPEs should not be directly connected in series or in parallel, and second, the total circuit impedance should be capacitive in the high-frequency limit and resistive in the low-frequency limit, as the impedance of an ionic conductor is expected to be as such. Any attempt to include more elements in the circuit than those dictated by the number of arcs in the spectrum will result in over-parameterization of the equivalent circuit, and the consequent large ambiguities in the determined parameter values will render the fitting results immaterial.

There are four possible circuit configurations comprising two resistors and two CPEs that fulfil the above conditions [4] and constitute candidate subcircuits to be incorporated into the general equivalent circuit of Fig. 2. The four subcircuits are shown in Fig. 3. Provided that the included CPEs share a common exponent, it can be shown that the circuits exhibit identical impedance frequency response by an appropriate transformation of their elements' parameter values [1, 4]. In this sense, the four circuits are indistinguishable. In particular, circuits B and C exhibit identical frequency response even when the exponents of their CPEs are not equal. In order for a model equivalent circuit to be fitted to an experimental impedance spectrum that presents two semicircular arcs, any of the four subcircuits of Fig. 3 would technically suffice to model the sample properties, at least as a first approximation. Of course, if the constraint that the exponents of the two CPEs should be equal is lifted, that is, they are allowed to vary independently during fitting, the impedance response of the circuits is not identical in a strict mathematical sense, although it remains qualitatively the same in the context that the two semicircles in the Nyquist plot are always present. Given the different impedance response in case of unequal CPE exponents, it could be suggested that, in principle, it may be possible to discriminate equivalent circuits on the basis of time constants. However, this problem has not been theoretically addressed due to the complicated mathematical calculations required. Analytical expressions of time constants are known only for the simple configuration of a CPE and a resistor in parallel connection [1] and can therefore be approximately applied to both such components of circuit A, provided that the time constants happen to be well resolved. Nevertheless, it seems by experience that time constants depend weakly on CPE exponents. In practice, taking into account the closely matched impedance response of the four alternative circuits in Fig. 1, implying closely similar time constants, along with the ubiquitous experimental errors of impedance data points, we may state that it does not seem possible to discriminate circuits by analysing time constants.

The solid lines accompanying data points in the typical impedance spectrum shown in Fig. 1 represent the best fitted frequency response according to each one of the four circuits of Fig. 3. The respective equivalent circuit parameter values are listed in Table 1. We must note here that, according to the usual definition of the CPE [1], the unit of measurement of the pre-exponential factor depends on the value of the exponent. To overcome this ambiguity, we have used a slightly different equation to define the CPE, which numerically coincides with the equation found in the literature [1]. The impedance of the CPE, which will be denoted as Q hereafter, is given by

$$Z_Q(\omega) = \frac{1}{Y\left(j\frac{\omega}{\omega_0}\right)^n} \quad (1)$$

where ω is the angular frequency, the pre-exponential factor Y is measured in conductance units (S) and is equal to the

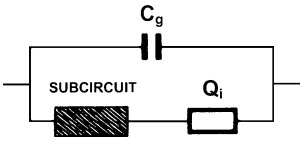

Fig. 2 General equivalent circuit of the experimental cell intended for impedance measurements

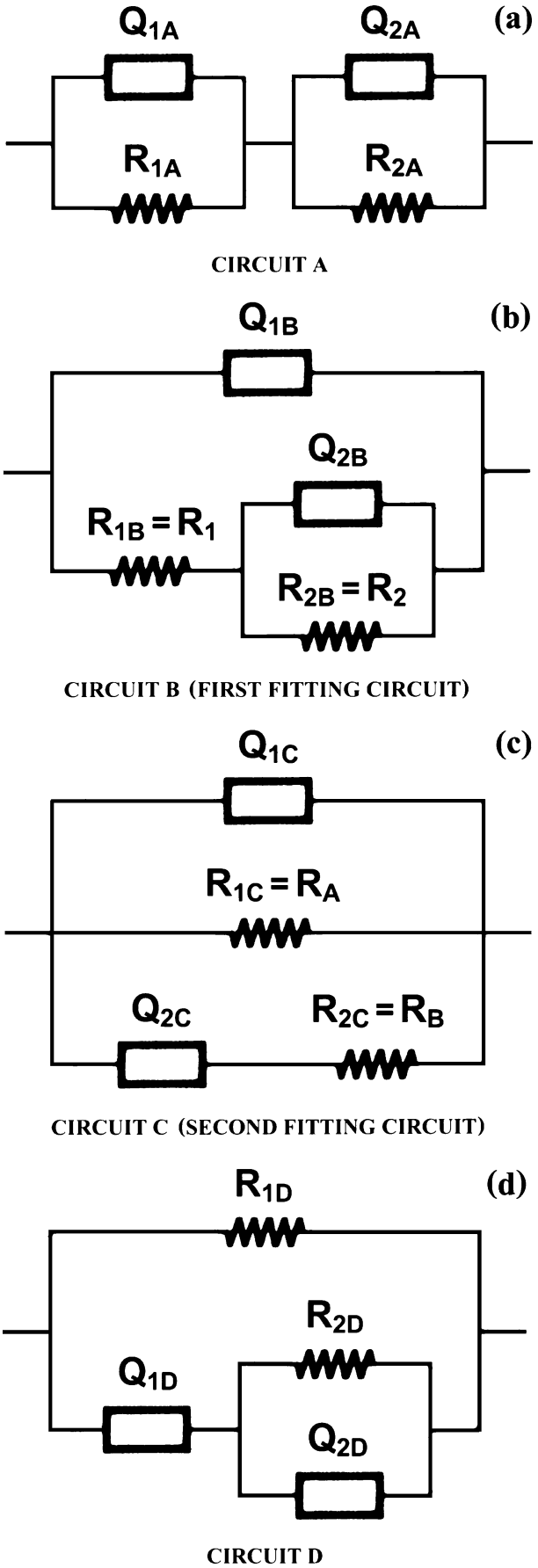

◀ **Fig. 3** Equivalent circuits exhibiting identical impedance frequency response with two semicircular arcs in the Nyquist plot (specific cases of the degenerate circuits contained in [4])

CPE's admittance modulus at angular frequency $\omega_0 = 1$ rad/s, j is the imaginary unit, and the possible values of the exponent n are limited in the interval $0 < n < 1$.

It is evident that the difference in the simulated total impedance according to the predictions of the four circuits is only marginal and, qualitatively, essentially the same. In practice, one of the subcircuits will provide the best fitted sum of squares, but this fact, in any case, does not provide a safe criterion of choice among them, as the experimental errors associated with the measured data points may introduce greater uncertainty in the merit of the fitted response than the inherent ambiguity that is related to the marginally different response of the candidate circuits. The choice of the most appropriate circuit model will be based on physical reasoning.

Comparison of equivalent circuits

The circuit that is usually adopted as a model for a two-phase material is circuit A of Fig. 3, largely because it offers a straightforward correspondence of its elements to the graphical components of the impedance Nyquist plot [1–3], which allows proper initialization of the circuit parameters for data fitting. However, from a structural point of view, the topology of circuit A implies that the two phases in the material are stacked in consecutive parallel layers, an assumption that is not at all realistic [5]. The configuration of a CPE and a resistor connected in parallel constitutes the standard electrical model of a homogeneous, single-phase ionic conductor [1]. The resistor models the DC resistance of the ionic conductor, as the transport of mobile ions dominates the total impedance response in the low-frequency limit. The CPE models the conductivity and/or dielectric relaxation processes [1, 32, 33] that give rise to the experimentally observed non-ideal capacitive impedance response of the ionic conductor in the high-frequency limit.

If circuit A is adopted as the two-phase material model, the two CPEs should represent the electrical relaxation processes occurring within the two individual, distinctly separated constituent phases. Besides the structural implications that have already been mentioned, another disadvantage of circuit A is set by the relative magnitude of the conductance, or non-ideal capacitance, of the circuit CPEs as yielded by experimental data analysis. The results contained in Table 1 indicate that the non-ideal capacitance of these two CPEs differs by three orders of magnitude. If, according to circuit A, these capacitance values are

Table 1 Computed parameters of the four alternative circuits of Fig. 3, incorporated into the general equivalent circuit of Fig. 2 and fitted to the experimental impedance spectrum of Fig. 1

Circuit	Y_1 (S)	n_1	R_1 (MΩ)	Y_2 (S)	n_2	R_2 (MΩ)	Y_i (S)	n_i
A	5.72×10^{-11}	0.876	2.63	1.97×10^{-8}	0.623	1.45	5.46×10^{-7}	0.535
B	5.30×10^{-11}	0.878	2.74	2.25×10^{-8}	0.627	1.34	5.46×10^{-7}	0.536
C	5.30×10^{-11}	0.878	4.08	2.43×10^{-9}	0.627	8.34	5.46×10^{-7}	0.536
D	1.17×10^{-9}	0.736	3.92	6.84×10^{-11}	0.879	7.45	5.11×10^{-7}	0.497

attributed to the conductivity and/or dielectric relaxation response of the two phases, such a large difference in magnitude would be understandable by a corresponding difference in the thickness of each phase layer. However, so large a difference in the coverage of the total material volume by the two phases is not the case [5]. On the other hand, as can be seen in the figures of Table 1, the yielded values of the modulus, as well as the exponent, of the second CPE in the equivalent circuit, the one designated at lower frequencies, bear a closer resemblance to the respective parameters of CPE Q_i, which models the impedance of the interfaces between the sample and the electrodes. This observation provides a hint as to the more likely origin of the second CPE in the equivalent circuit: the interfacial impedance of the rough boundary surfaces separating the dispersed crystalline grains from the bulk vitreous phase. The following revision of the equivalent circuit will be directed by the above observation.

The anticipated high-frequency response of any ionic conductor indicates that the equivalent circuit should include a CPE, directly connected between the circuit ends, to model the material high-frequency conductivity and/or dielectric relaxation processes. Any other elements, arranged in no matter which way, should be connected to this CPE in parallel. The underlying assumption is that the high-frequency limiting behaviour of the dielectric function of the two constituent phases is similar, an approximation that is reasonable from a numerical point of view [1]. The introduction of such a simplification becomes a pragmatic necessity, taking into account the ever-present constraint that experimental data fitting is unambiguous if two resistors and two CPEs only are included in the circuit.

Circuits B and C of Fig. 3 meet the above requirement, whereas circuit D does not, and for this reason, it is rejected. The topology of circuit D implies that the interfacial phenomena occurring at the boundaries between phases and the bulk high-frequency relaxation processes are activated in sequence. Hence, bearing in mind its inefficiency to account for the material microstructure and the correlated current flow mechanisms, the fact that this circuit always provides the worst fitting sum of squares might not be incidental.

The choice between circuits B and C will depend on the interconnection of the rest of the elements and the association of each element with a particular electrical response process. Circuit B successfully accounts for the structure of the phases making up the material. Resistor R_{1B} corresponds to long-range conduction of ions through the vitreous phase, which constitutes the background in which suspended grains of the crystalline phase are scattered. On the interfaces that separate the two phases, the ionic current is divided into two components, one that is capacitively blocked, and its frequency dispersion is modelled by CPE Q_{2B}, and another that crosses the interface and its path is modelled by resistor R_{2B}, which accounts for the anticipated different ionic conductivity of the two phases and the dimensions of the grains.

The difference between the topologies of circuits B and C is that, according to circuit C, the two components of the ionic current are distinctly separated throughout the sample volume, all the way through, from one current-collecting electrode to the other, as if extensive, well-defined portions of the interfaces exist, which either block or allow the ionic current to cross. What is more, resistor R_{1C}, which is connected directly to the circuit ends, should be the sum of two contributions in series, namely, conduction through the vitreous and through the crystalline phase, one followed by the other. As these two long-range conduction processes are expected to be thermally activated by different activation energies, this resistor should vary with temperature in a non-Arrhenius manner.

We conclude that circuit B, among the circuits of Fig. 3, is the most appropriate to model the impedance properties of two-phase ionic conductors. However, the configuration of circuit B implies that, on application of voltage to the experimental cell, every ionic carrier that migrates through the ionic conductor from one end to the other encounters at least one interface separating crystalline grains from the vitreous background of the material structure. This electrical conduction scheme is definitely not sufficient to describe current flow in case the density of the dispersed crystalline islands in the vitreous phase is low enough to permit the existence of current conduction paths that cross the sample from one end to the other without passing through any parts of the crystalline phase. Circuit B, then, has to be revised to include the possibility of conduction through one of the constituent phases only and not exclusively through both the phases.

Description of the model

Before describing the model, it is necessary to make some simplifying assumptions concerning the structural properties of the solid two-phase material, as well as the flow of ionic drift current through the system. The two-phase material is composed of a continuous vitreous background phase in which crystalline grains are dispersed [5]. This configuration in the micrometer scale structure is demonstrated in the scanning electron microscopy pictures shown in the second part of this work. The vitreous and crystalline phases are supposed to be homogeneous. The individual grains of the crystalline phase are characterized by identical electrical properties. We assume that the current flow lines are parallel to each other and normal to the planar current-collecting ohmic contacts that have been formed on either side of the sample. We also assume that there is no fringing of the current flow lines round the crystalline grains. The interfaces separating the grains from the vitreous background are ideally thin; that is, any boundary interphase between the grains and the background has not been formed. The ionic charge carriers that cross the interfaces are not hindered by any additional electrical impedance due to the discontinuity in the material structural properties that exists at the interfaces. In summary, the assumptions regarding the structure of the material (homogeneous phases, identical grain properties, absence of any interphase formed between the two phases) are introduced to the purpose of excluding the otherwise possible appearance of additional relaxations in the impedance response. On the other hand, the supposed properties of current flow lines (being parallel, without any fringing) contribute to simplicity in modelling the effects of geometry on impedance properties. For example, complete fringing of current flow lines round small grains would imply bypassing conduction effects in the crystalline phase. In consequence, the presence of the crystalline grains in the material would not affect the impedance response.

The proposed equivalent circuit model of a two-phase solid state ionic conductor is shown in Fig. 4. It consists of three parallel branches, each of which corresponds to one of the three macroscopically differentiated conduction processes that can be initiated on application of an electric stimulus to the sample. The first branch, comprising a single CPE denoted as Q_V, models the frequency response of the bulk conductivity and/or dielectric relaxation mechanisms of mobile ions and bound dipole charges, respectively. This branch dominates the total impedance behaviour of the equivalent circuit at high frequencies. The second branch is more complex and models the frequency response of the long-range conduction current of mobile ions, the path of which passes through parts of both the vitreous and the crystalline phases. Resistors R_V and R_C

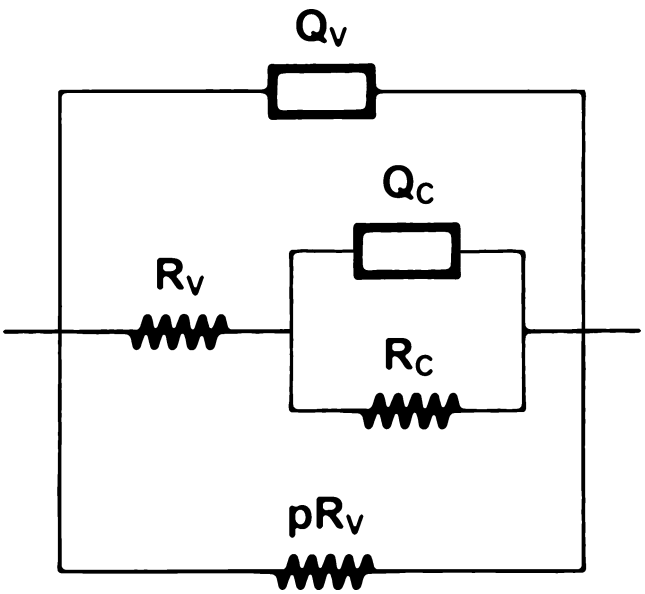

Fig. 4 The proposed equivalent circuit model of a two-phase ionic conductor

stand for the total DC resistance that the vitreous and crystalline phase, respectively, exhibit to the flow of ionic current. The above resistance values correspond to a fraction of the total sample volume; the cross-section of which, with respect to the direction of current flow, includes all possible paths that involve passage of ionic carriers through crystalline grains. The second CPE in the circuit, denoted as Q_C, models the impedance response of the interfaces between the crystalline grains and the vitreous background. The parallel connection of Q_C and R_C implies that the ionic charge carriers are visualized as being partly blocked at the interfaces between the two phases. On application of voltage, a fraction of the ions drifted to interfaces are accumulated to form interfacial double layers, whereas the rest cross the interfaces to continue long-range conduction in both the phases on either side of each interface. Finally, the third branch of the equivalent circuit comprises a single resistor pR_V and models the components of the ionic current, the paths of which from one current-collecting electrode to the other do not cross any crystalline grains, thus, involving long-range conduction exclusively through the vitreous phase. The resistance of this resistor corresponds to the rest of the total sample volume, the cross-section of which, with respect to the direction of current flow, includes all possible paths through the vitreous phase only, and for this reason, it is set proportional to the resistance of resistor R_V of the second branch by introducing a numerical parameter, denoted as p. This parameter is expected to depend on the geometrical features of the material microstructure, and not on temperature, as resistors R_V and pR_V of the second and third branch, respectively, should vary with temperature follow-

ing the Arrhenius equation by the same activation energy, which is a characteristic property of the vitreous phase. The capacitive response, coupled to the ohmic ionic transport process represented by pR_V, is modelled by the first CPE, Q_V. Obviously, the third branch should not be included in the equivalent circuit in case the grains are so densely scattered throughout the sample volume, that there is no net conduction path solely through the vitreous phase.

Model implications

The addition of a third resistor in the model of Fig. 4 results in over-parameterization of the equivalent circuit that is to be fitted to impedance spectra measured from real two-phase materials. Consequently, data analysis by directly incorporating the model into the general equivalent circuit of Fig. 2 is not feasible, at least as far as the aspect of numerical computations is concerned. However, the model of Fig. 4 exhibits identical impedance frequency response with circuits B and C of Fig. 3. From now on, these circuits will be referred to as the first and second fitting circuit, respectively. Furthermore, to simplify the notation of the equations that will be presented below, the ohmic elements of the fitting circuits have been conveniently renamed as shown in Fig. 3. Experimental data fitting can be unambiguously carried out by including either one of the two alternative subcircuits of Fig. 3b,c into the general equivalent circuit. Of course, as has been demonstrated in Fig. 1, data fitting may as well be accomplished by alternatively adopting circuits A and D of Fig. 3a,d as the two-phase material model, although they are not strictly equivalent to the proposed circuit model of Fig. 4. The problem of physical interpretation of the elements, as well as the topology, of each one of the circuits of Fig. 3, which has been discussed in the previous sections, has settled to the conclusion that using circuits B and C for experimental data fitting is advantageous in comparison to circuits A and D. A further matter that arises is decoupling the physical information, conveyed by the parameters of the proposed model, from the parameters of the fitting circuits, which out of computational necessity are simpler than the model. This problem will now be addressed in terms of interpreting and analysing the temperature dependence of the fitting circuits' parameters by employing computer simulations. Our discussion is confined to ohmic elements only to investigate the variation of ionic conductivity with temperature in two-phase materials, depicted in Arrhenius plots. Although we will be dealing exclusively with the fitting circuits of Fig. 3b and c, a corresponding behaviour is observed in the Arrhenius plots of the fitting parameters in case circuits A and D of Fig. 3a,d are adopted as the material circuit model.

Relations between the fitting circuits' elements and model parameters can be established by mathematical investigation [4]. The correspondence of the used symbols to circuit elements is explained in Figs. 3b,c and 4. Physical meaning of model parameters has been described in the previous section. The equations derived are

$$R_1 = \frac{p}{p+1} R_V \tag{2}$$

$$R_2 = \left(\frac{p}{p+1}\right)^2 [(p+1)R_V // R_C] \tag{3}$$

for the first and

$$R_A = (R_V + R_C) // pR_V \tag{4}$$

$$R_B = \frac{R_V}{R_C}(R_V + R_C) \tag{5}$$

for the second fitting circuit. In the above equations, $R_i // R_j$ signifies the parallel combination of resistors R_i and R_j, that is,

$$\frac{1}{R_i // R_j} = \frac{1}{R_i} + \frac{1}{R_j} \tag{6}$$

Let $G_i = R_i^{-1}$ be the conductance of resistor R_i in an equivalent circuit. We assume that the ionic conductivity in both the vitreous and the crystalline phases obeys the classic Arrhenius law with different activation energy, which we denote as E_V and E_C, respectively. As, according to the proposed model, the macroscopic conductances G_V and G_C are expected to be related to the respective phase conductivities through geometrical microstructural parameters only, it follows that they, too, should obey the Arrhenius equation by the same activation energies,

$$G_V = \frac{1}{R_V} = F_V \exp\left(-\frac{E_V}{kT}\right) \tag{7}$$

$$G_C = \frac{1}{R_C} = F_C \exp\left(-\frac{E_C}{kT}\right) \tag{8}$$

where F_V and F_C are the corresponding conductance pre-exponential factors, T is the absolute temperature and k is Boltzmann's constant.

If Eqs. 7 and 8 are inserted into Eqs. 2 and 3, the temperature dependence of conductances G_1 and G_2 of the first alternative fitting circuit may be calculated and the corresponding Arrhenius plots constructed. In the same way, by substituting Eqs. 7 and 8 into 4 and 5, the

respective temperature dependence of conductances G_A and G_B of the second alternative fitting circuit and the associated Arrhenius plots can be derived.

The results of computer simulations of the Arrhenius plots, obtained by the above procedure, are shown in Figs. 5, 6, and 7. The temperature range covered is 250 to 1,000 K. Reasonable values of pre-exponential factors, activation energies and parameter p have been selected to model the electrical properties of the two constituent phases in the proposed equivalent circuit, and they are listed in the legends of the corresponding figures. The resulting variation in the shape of each Arrhenius plot, caused by altering the relative magnitude of pre-exponential factors, activation energies of the phases and parameter p are shown in Figs. 5, 6 and 7, respectively.

It is evident that, with the exception of conductance G_1 of the first fitting circuit, non-Arrhenius behaviour is observed in the temperature dependence of the fitting circuits' ohmic elements G_2, G_A and G_B. Each Arrhenius plot exhibits dual slope, tending asymptotically to a straight line in the low and high-temperature limits, with a transition region in the intermediate temperature range. The slope of every Arrhenius plot in the low-temperature limit corresponds to the vitreous phase activation energy, although in some cases, when the activation energies of the two phases are similar or parameter p takes large values, this low-temperature limiting slope shifts to temperature ranges beyond the extent of customary experimental conditions. On the contrary, the slope of the asymptote straight line in the high-temperature limit depends on the activation energy of both the phases, in different manners for each plot. The conditions that should be fulfilled in order for the Arrhenius plots to exhibit dual slope in the useful temperature range covered in experimental investigations are: (1) The conductance pre-exponential factors should differ by many orders of magnitude, (2) the activation energies of the two phases should also differ appreciably, and (3) parameter p should not take extremely small or extremely large values. Only qualitative descriptions of the previous conditions have been given intentionally, as the extent to which each one of them holds affects the extent of the others. For instance, larger difference in activation energies will result in smaller relative magnitude of pre-exponential factors so as for the dual slope to appear in the Arrhenius plots. Exact

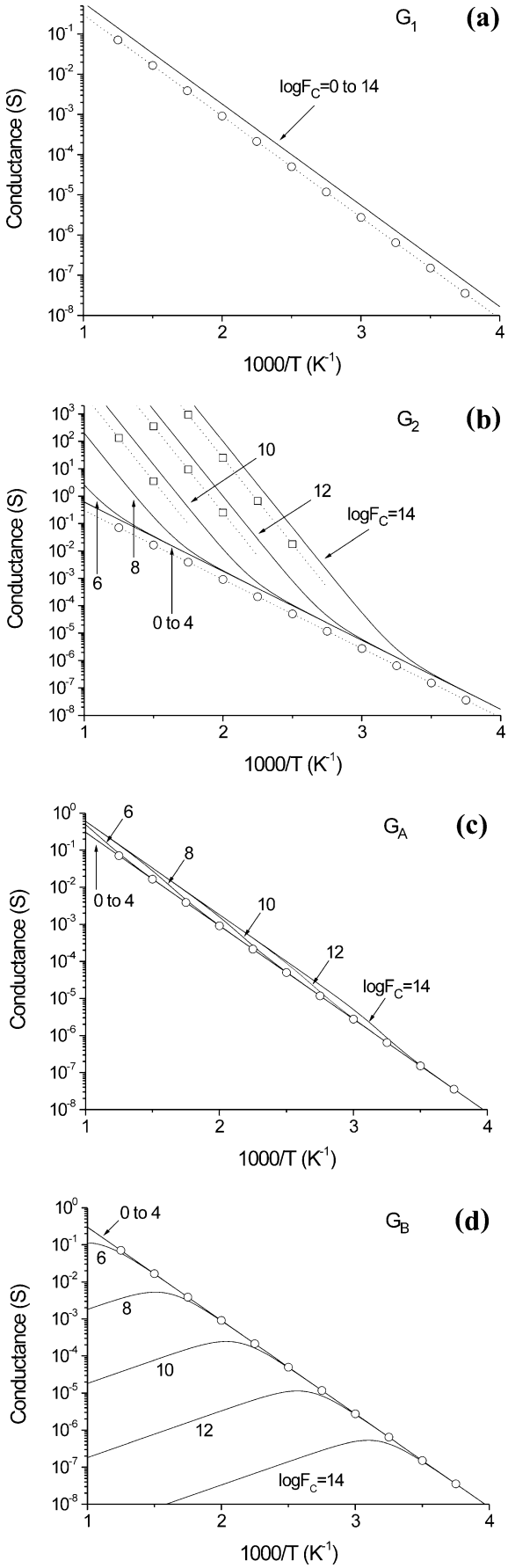

Fig. 5 Simulated Arrhenius plots of the ohmic elements G_1 (**a**), G_2 (**b**), G_A (**c**) and G_B (**d**), of the fitting circuits of Fig. 3b,c, corresponding to crystalline phase conductance pre-exponential factor ranging from $F_C=1$ S to $F_C=10^{14}$ S. The other model parameters used are $E_V=0.5$ eV, $E_C=1.25$ eV, $F_V=10^2$ S and $p=1$. The *open circles* and *squares*, respectively, accompanied by *dotted lines*, represent the temperature dependence of conductances G_V and G_C in the model of Fig. 4. They are displayed, wherever necessary, to indicate the low and/or high-temperature limiting behaviour of the slope of the simulated curves

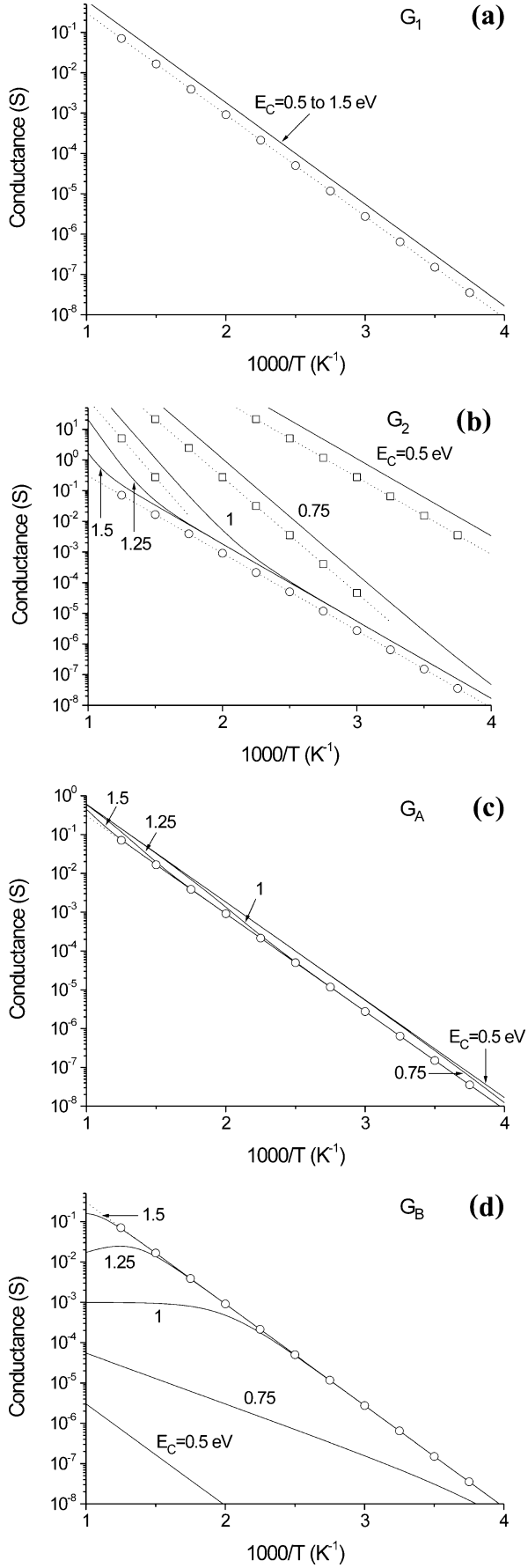

◀ **Fig. 6** Simulated Arrhenius plots of the ohmic elements G_1 (**a**), G_2 (**b**), G_A (**c**) and G_B (**d**), of the fitting circuits of Fig. 3b,c, corresponding to crystalline phase activation energy ranging from E_C=0.5 eV to E_C=1.5 eV. The other model parameters used are E_V= 0.5 eV, $F_V=10^2$ S, $F_C=10^7$ S and p=1. The *open circles* and *squares*, respectively, accompanied by *dotted lines*, represent the temperature dependence of conductances G_V and G_C in the model of Fig. 4. They are displayed, wherever necessary, to indicate the low and/or high-temperature limiting behaviour of the slope of the simulated curves

quantitative conclusions can be drawn with the aid of the following mathematical calculations.

It is possible to extract analytical expressions describing the Arrhenius plots of the ohmic elements of the fitting circuits of Fig. 3b,c. In the next paragraphs, we adopt the following notation. Arrhenius plots are described as equations relating the respective ordinate variable y_i to a common abscissa variable x. The subscript of each separate ordinate variable refers to the corresponding fitting circuit parameter depicted in the Arrhenius plot. Thus, subscripts 1, 2, A, B and AB correspond to Arrhenius plots of conductances G_1, G_2, G_A, G_B and G_A+G_B, respectively. Furthermore, to describe the asymptotes of Arrhenius plot curves, superscripts 0 and ∞ are used to refer to the asymptote in the low and high temperature limit, respectively.

As far as the first fitting circuit is concerned, taking into account that the abscissa and ordinate variables of an Arrhenius plot are $x=10^3$ T^{-1} and y_i=logG_i, respectively, and substituting Eqs. 7 and 8 into 2 and 3, after some algebraic manipulation, we obtain

$$y_1 = \log G_1 = \log\left(\frac{p+1}{p}F_V\right) - \frac{E_V \cdot \log e}{10^3 k}\cdot x \tag{9}$$

and

$$y_2 = \log G_2 = \log\left(\frac{p+1}{p^2}F_V\right) - \frac{E_V \cdot \log e}{10^3 k}\cdot x + \log\left\{1+\exp\left[\ln\left((p+1)\frac{F_C}{F_V}\right) - \frac{E_C - E_V}{10^3 k}\cdot x\right]\right\} \tag{10}$$

where e is the base of natural logarithms.

It is also possible to derive analytical expressions of the asymptotes of the curve of Eq. 10 formed by conductance G_2 data points. In the low-temperature limit, where T<< $(E_C-E_V)/k$, Eq. 10 reduces to

$$y_2^0 = \log G_2^0 = \log\left(\frac{p+1}{p^2}F_V\right) - \frac{E_V \cdot \log e}{10^3 k}\cdot x \tag{11}$$

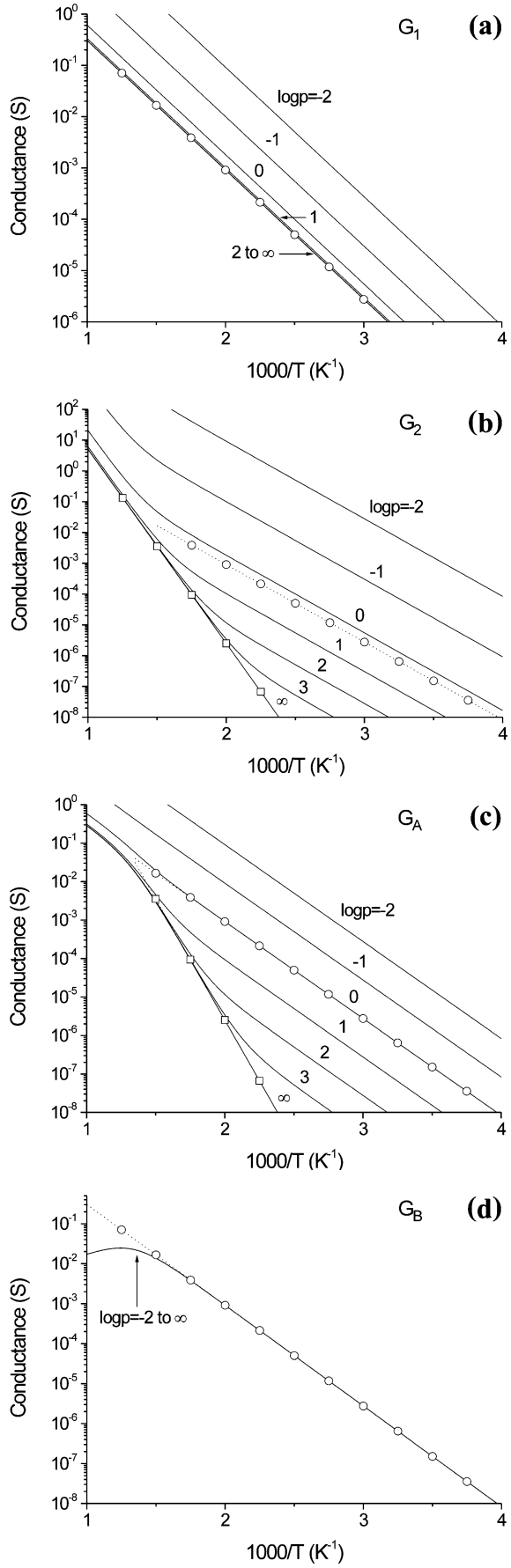

◀ **Fig. 7** Simulated Arrhenius plots of the ohmic elements G_1 (**a**), G_2 (**b**), G_A (**c**) and G_B (**d**), of the fitting circuits of Fig. 3b,c, corresponding to parameter p values ranging from $p=10^{-2}$ to $p=10^3$ and $p\to\infty$. The other model parameters used are $E_V=0.5$ eV, $E_C=1.25$ eV, $F_V=10^2$ S and $F_C=10^7$ S. The *open circles* and *squares*, respectively, accompanied by *dotted lines*, represent the temperature dependence of conductances G_V and G_C in the model of Fig. 4. They are displayed, wherever necessary, to indicate the low and/or high-temperature limiting behaviour of the slope of the simulated curves

Likewise, in the high-temperature limit, where $T>>(E_C-E_V)/k$, we obtain

$$y_2^{\infty}=\log G_2^{\infty}=\log\left\{\frac{p+1}{p^2}\left[F_V+(p+1)F_C\right]\right\}-\frac{E_VF_V+(p+1)E_CF_C}{F_V+(p+1)F_C}\cdot\frac{\log e}{10^3k}\cdot x \qquad (12)$$

If $F_C>>F_V$, an assumption justified by the provisos that must be met in order for the dual slope to appear in the Arrhenius plot, the above equation reduces to

$$y_2^{\infty}=\log G_2^{\infty}\cong\log\left[\left(\frac{p+1}{p}\right)^2F_C\right]-\frac{E_C\cdot\log e}{10^3k}\cdot x \qquad (13)$$

Furthermore, in the special case that p tends to infinity, that is, the crystalline islands are so densely dispersed in the vitreous material background that there is no clear ionic conduction path through the vitreous phase alone, Eq. 10 is simplified into

$$y_2=\log G_2\cong\log F_C-\frac{E_C\cdot\log e}{10^3k}\cdot x \qquad (14)$$

To summarize the predictions of the proposed model so far, we conclude that, when drawn in Arrhenius plots, conductance G_1 data points should always be lined up along a straight line, whereas conductance G_2 data points should be lined up along a curve, which asymptotically tends to two straight lines in the low-temperature and the high-temperature limits. The slope of the low-temperature asymptote should be equal to the slope of conductance G_1 data points' straight line. The ionic conductivity activation energy in the vitreous and the crystalline phase may be calculated from the slope of conductance G_1 straight line, which coincides with the slope of conductance G_2 low-temperature asymptote, and the slope of the G_2 high-temperature asymptote, respectively. In the special case of a two-phase material containing very densely scattered crystalline grains, both conductance G_1 and G_2 data points should be aligned along straight lines, the slopes of which determine the ionic conduction activation energy in the vitreous and crystalline phase, respectively.

As far as the second fitting circuit is concerned, the ionic conductivity activation energy in each phase, along with other model parameters, may be derived as well by employing a similar analysis. Despite the fact that, as is

evident from Eqs. 4 and 5, conductances G_A and G_B are both dependent on the properties of the vitreous as well as the crystalline phase, it is found that

$$G_A + G_B = \frac{p+1}{p} G_V \tag{15}$$

and, therefore, the vitreous phase activation energy may be calculated from the slope of the Arrhenius plot of the sum G_A+G_B.

Substituting Eqs. 7 and 8 into 4 and 5, the analytical expressions describing the corresponding Arrhenius plots are obtained,

$$y_{AB} = \log(G_A + G_B) = \log\left(\frac{p+1}{p} F_V\right) - \frac{E_V \cdot \log e}{10^3 k} \cdot x \tag{16}$$

and

$$y_B = \log G_B = \log F_V - \frac{E_V \cdot \log e}{10^3 k} \cdot x - \log\left\{1 + \exp\left[\ln\left(\frac{F_C}{F_V}\right) - \frac{E_C - E_V}{10^3 k} \cdot x\right]\right\} \tag{17}$$

The equations describing the low-temperature and high-temperature asymptotes of the curve of Eq. 17 that is formed by conductance G_B data points are

$$y_B^0 = \log G_B^0 = \log F_V - \frac{E_V \cdot \log e}{10^3 k} \cdot x \tag{18}$$

and

$$y_B^\infty = \log G_B^\infty = \log\left(\frac{F_V^2}{F_V + F_C}\right) - \frac{E_V(F_V + 2F_C) - E_C F_C}{F_V + F_C} \cdot \frac{\log e}{10^3 k} \cdot x \tag{19}$$

Because, as stated before, F_C>>F_V, Eq. 19 reduces to

$$y_B^\infty = \log G_B^\infty \cong \log\left(\frac{F_V^2}{F_C}\right) - \frac{(2E_V - E_C) \cdot \log e}{10^3 k} \cdot x \tag{20}$$

The conclusions drawn by the above equations are similar to the previous ones. The data points of the sum of conductances G_A+G_B should be lined up along a straight line, the slope of which allows calculation of the vitreous phase activation energy E_V. Conductance G_B data points should be lined up along a curve, which again tends asymptotically to two straight lines in the low-temperature and the high-temperature limits. The slope of the low-temperature asymptote should be equal to the slope of the straight line, along which data points of the sum G_A+G_B are aligned. The differentiation in analysis results, in comparison to the previous case of data returned by the first fitting circuit, is that the slope of the high-temperature asymptote is determined not by the crystalline phase activation energy E_C alone, but by the factor $2E_V$−E_C. It is interesting that if E_C>$2E_V$, the slope of the high-temperature asymptote is found to be positive; that is, conductance G_B decreases with increasing temperature. Such is the case in the simulated Arrhenius plots of Fig. 5.

Despite the fact that data fitting may be performed equally well with either one of the two fitting circuits of Fig. 3b and c, use of the first one is preferable for the simple reason that, when parameter p tends to infinity, its resistors are directly related to the ionic conductivity of the two material phases. In this particular case, the third branch pR_V should not be included in the proposed equivalent circuit model.

Conclusions

The equivalent circuit of Fig. 4 is proposed as a model to account for the impedance properties of two-phase solid state ionic conductors. The materials suitable for application of the model should conform to a particular microstructure, according to which one of the phases, the crystalline in the given typical example, is dispersed in the form of isolated islands within the background of the other phase, the vitreous in the example. The topology of the equivalent circuit is considered to be the most appropriate to adequately describe the interrelation of the electrical response processes occurring during ionic current flow within the two-phase material sample.

Two alternative equivalent circuits, shown in Fig. 3b and c, are proposed to carry out experimental impedance data fitting, obtained from real two-phase materials as a function of temperature. Owing to the fact that the fitting circuits are simpler than the model circuit, a modified analysis procedure of the resulting Arrhenius plots was developed to derive the microscopic electrical properties of the constituent material phases. Impedance spectra, recorded at various temperatures, may be fitted to either the first or, alternatively, the second of the fitting circuits of Fig. 3b and c, respectively. The returned resistance values of the ohmic elements R_1, R_2 or R_A, R_B of the two circuits are then converted to the respective conductance values G_1, G_2 or G_A, G_B. Finally, G_1 and G_2, or G_A+G_B and G_B, are plotted against the inverse of temperature to construct the Arrhenius plots.

According to the implications of the proposed model, the slope of conductance G_1 Arrhenius plot, as well as of the low-temperature asymptote of conductance G_2 plot, is directly related to the activation energy E_V of the vitreous phase. The slope of the high-temperature asymptote of the G_2 plot is directly related to the activation energy E_C of the

crystalline phase. Likewise, the slope of the sum G_A+G_B Arrhenius plot, as well as of the low-temperature asymptote of the G_B plot, is directly related to E_V, whereas the slope of the high-temperature asymptote of the G_B plot is dependent upon the factor $2E_V-E_C$. In any case, whether the first or the second alternative fitting circuit is used for experimental data analysis, it is feasible to derive the activation energies of the individual phases making up the material.

In the limiting structural configuration of the two-phase material, where the islands of the crystalline phase are very densely distributed within the vitreous phase, the model circuit of Fig. 4 becomes simplified and coincides with the first fitting circuit of Fig. 3b. When such is the case, both the G_1 and G_2 Arrhenius plots reduce to straight lines, the slope of which is directly related to E_V and E_C, respectively.

Acknowledgements This work has been supported by the Greek Ministry of Education through the Pythagoras II research programme.

References

1. Macdonald JR (ed) (1987) Impedance spectroscopy emphasizing solid materials and systems. Wiley, New York
2. Julien C, Nazri GA (1994) Solid state batteries: materials design and optimization. Kluwer, Boston
3. Balkanski M (ed) (1991) Microionics: solid state integrable microbatteries. North-Holland, Amsterdam
4. Fletcher S (1994) J Electrochem Soc 141:1823
5. Horopanitis EE, Perentzis G, Pavlidou E, Papadimitriou L (2003) Ionics 9:88
6. Tuller HL, Button DP, Uhlmann DR (1980) J Non-Cryst Solids 40:93
7. Tatsumisago M, Yoneda K, Machida N, Minami T (1987) J Non-Cryst Solids 95–96:857
8. Thangadurai V, Schwenzel J, Weppner W (2005) Ionics 11:11
9. Lilley E, Strutt JE (1979) Phys Status Solidi A 54:639
10. Näfe H (1984) Solid State Ionics 13:255
11. De Jonghe LC (1979) J Mater Sci 14:33
12. Kincs J, Martin SW (1996) Phys Rev Lett 76:70
13. Ribes M, Taillades G, Pradel A (1998) Solid State Ionics 105:159
14. Ngai KL, Rizos AK (1996) Phys Rev Lett 76:1296
15. Macdonald JR (1998) J Appl Phys 84:812
16. Martin SW, Martin DM, Schrooten J, Meyer BM (2003) J Phys Condens Matter 15:S1643
17. Bauerle JE (1965) J Phys Chem Solids 30:2657
18. Hodge IM, Ingram MD, West AR (1976) J Electroanal Chem 74:125
19. Beekmans NM, Heyne L (1976) Electrochim Acta 21:303
20. Van Dijk T, Burggraaf AJ (1981) Phys Status Solidi A 63:229
21. Verkerk MJ, Middlehuis BJ, Burggraaf AJ (1982) Solid State Ionics 6:159
22. Dygas JR, Fafilek G, Breiter MW (1999) Solid State Ionics 119:115
23. Schouler EJL, Mehabi N, Vitter G (1983) Solid State Ionics 9–10:989
24. Sku EM, Jacobsen T (1989) Appl Phys A 49:117
25. Fleig J, Maier J (1999) J Am Ceram Soc 82:3485
26. Abram EJ, Sinclair DC, West AR (2003) J Electroceram 10:165
27. Huggins RA (2002) Ionics 8:300
28. Scheider W (1975) J Phys Chem 79:127
29. Liu SH (1985) Phys Rev Lett 55:529
30. Kerner Z, Pajkossy T (1998) J Electroanal Chem 448:139
31. Song HK, Jung YH, Lee KH, Dao LH (1999) Electrochim Acta 44:3513
32. Funke K (1986) Solid State Ionics 18–19:183
33. Macdonald JR (1997) J Non-Cryst Solids 197:83